Journal of
Composites Science

MDPI

Article

Modelling and Experimental Investigation of Hexagonal Nacre-Like Structure Stiffness

Rami Rouhana [1,*] and Markus Stommel [2]

[1] Chair of Plastics Technology, TU Dortmund University, Leonhard-Euler-Str. 5, 44227 Dortmund, Germany
[2] Leibniz Institute of Polymer Research, Hohe Str. 6, 01069 Dresden, Germany; stommel@ipfdd.de
* Correspondence: rami.rouhana@tu-dortmund.de

Received: 26 June 2020; Accepted: 11 July 2020; Published: 15 July 2020

Abstract: A highly ordered, hexagonal, nacre-like composite stiffness is investigated using experiments, simulations, and analytical models. Polystyrene and polyurethane are selected as materials for the manufactured specimens using laser cutting and hand lamination. A simulation geometry is made by digital microscope measurements of the specimens, and a simulation is conducted using material data based on component material characterization. Available analytical models are compared to the experimental results, and a more accurate model is derived specifically for highly ordered hexagonal tablets with relatively large in-plane gaps. The influence of hexagonal width, cut width, and interface thickness are analyzed using the hexagonal nacre-like composite stiffness model. The proposed analytical model converges within 1% with the simulation and experimental results.

Keywords: nacre; stiffness; hexagonal tablets; analytical model; finite element simulations; composite; Abaqus

1. Introduction

Nature presents several structures optimized through evolution. Nacre is currently a central inspiration for biomimetic structure design and manufacturing methods for toughened ceramics, as showcased by Bouville [1]. Nacre consists of microscale tablets of brittle ceramic material assembled in brick mortar form and connected by a relatively tough binding organic material. Natural nacre consists of calcium carbonate bonded by protein molecules and polysaccharides [2]. This construction of overlapping tablets increases the toughness of the material by two orders of magnitude or more than bulk brittle material, as described by Bathelat et al. [3]. The most attractive feature in this construction is that it maintains considerable stiffness and strength, as measured by Wang et al. [4] and Currey [5]. This feature is becoming attractive to composite engineers for the development of novel composite types, which has been an active research area for the last two decades. Budarapu [6] further adds that the nacre structure resists crack propagation running across the tablets and main deformation of the structure, which is due to tablet sliding until pull-out.

Several methods at different scales have replicated the structure. At the macro-scale, constructed sheets are described in the work of Yin et al. 2019 [7] and Valashani and Barthelat [8], where millimeter-scale tablets were produced from laser cut glass sheets and were assembled using polymeric ethylene-vinyl acetate or polyurethane as matrix material, and then tested for side impact loads. Pre-preg fiber-reinforced sheets are cut into tiles and carefully assembled to overlap by half of their length in the work of Narducci and Pinho [9].

At the micro-scale, layers of reinforcing material are randomly assembled, or oriented/positioned with limited control. In the work of Grossman et al. [10], alumina tablets were magnetically oriented and bonded using polyetherimide (PEI) polymer as a matrix. Launey et al. [11] presented a method using ice-templating to produce a ceramic-metal composite with good mechanical properties. Another method

demonstrated at the micro-scale was described by Munoz et al. [12], which allows the manufacturing of high-toughness composite using a freeze-granulation method, in which 7-µm-diameter Alumina tablets were oriented by sedimentation and later sintered with silica as the matrix interface.

At the nanoscale, De Luca et al. [13] demonstrated the deposition of well-aligned sub-micron inorganic tablets of 90% weight percentage on the surface of glass fibers, improving the interfacial strength and energy dissipation by up to 30%. The processes developed in this study have different limitations, as they are complicated, time-consuming, non-scalable, have limited accuracy, and are difficult, as supported by the review of Mirkhalaf and Zreiqat [14]. Finally, the work of Wegst et al. [15] summarized the manufacturing methods and added the use of additive manufacturing methods for generating nacre-like structures as a potential path for future research.

The finite element method (FEM) has been used to estimate structure stiffness, energy absorption, and other mechanical properties with acceptable accuracy. In the work of Grujicic et al. [16], FEM was used to assess the impact damage of a rigid projectile on a nacre-like body armor structure consisting of Boron Carbide; at the millimeter scale, hexagonal tablets were bonded by polyuria matrix. The study concluded that a nacre-like structure had superior penetration resistance when compared to a monolithic structure. Raj et al. [17] used FEM to predict the toughness of a highly organized hierarchical structure of nacre consisting of calcium carbonate tablets bonded by an organic matrix with the work being in good agreement with experimental measurements. Li et al. [18] also made use of FEM to compare the predicted stiffness and strength of nacre-like tablets and compared them to experimentally produced specimens using an additive manufacturing method.

Analytical models have been developed for composite structures since the proposal of the rule of mixture model by Voigt [19] in 1889. This model, which depends on the volume quantities of the composite components, is accurate enough to estimate the stiffness of long fiber composites. Nacre structures are discontinuous reinforcement composites and thus have a non-uniform cross-section. However, if nacre structures are accurately assembled with a high length-to-thickness ratio, the structures behave as a continuous body and revert to the rule of mixture, while at the same time possessing in-plane isotropy, as explained by Kim et al. [20]. Models for nacre structures have been developed, but with several conditions and assumptions to accept their validity, as in the work of Kotha et al. [21]. Such models have several limitations and do not apply to certain geometries. Liu et al. [22] presented a model for analyzing the stress fields between the tablets at the nanoscale, concluding that a smaller aspect ratio of tablet size to thickness and a larger elastic modulus ratio between reinforcement and matrix led to a more uniform shear stress distribution in the matrix. Most studies presented here conclude that further analysis is still required to predict the mechanical properties of nacre-like structures accurately. Further improvement is needed for experimental methods to produce nacre-like composites and measure the mechanical properties of such structures; these statements are repeated in the work of Bonderer et al. [23], Miao et al. [24], Mirkhalaf et al. [25], and Luz and Mao [26].

The method presented in this work details the selection of two readily available materials that fit the criteria of nacre brittle/tough combination and can be processed by easily accessible tools. This simplification should allow for fast geometry development, leading to direct experimental validation, more accurate analytical models, and reliable simulation models. Polystyrene (PS) sheets are selected as the reinforcing component, with brittle behavior and relatively high stiffness. Polyurethane (PU) is chosen as the nacre matrix component due to its higher toughness and the fact that, as a liquid solution, it can be cast similarly to epoxy. The nacre geometry is laser cut from thin polystyrene sheets, and then several alternating layers are assembled to ensure optimum overlap. The polystyrene sheets are held together by interlayers of polyurethane solution. These assembled sheets have each component characterized mechanically, and then each assembled sheet is tested in tensile and has its stiffness measured. These composite sheets are then modeled in computer-aided design (CAD), following digital microscope measurements and simulated by Simulia/Abaqus (version 2017, Dassault Systemes, Vélizy-Villacoublay, France) [27] FEM software to determine the stiffness.

The measured and simulated values can then be compared to analytical models developed for nacre mechanical properties prediction and, in this specific case, stiffness. The analytical model presented by Padawer and Beecher [28] is to specifically predict the stiffness of nacre like structures with reinforcing tablets overlapping. The overlap of tablets causes increases in shear stresses of the structure. In the case of nacre-like assemblies, the shear modulus of the matrix material is an important variable in the mechanical performance of the composite. A third analytical model is presented by Lusis et al. [29] with a correction to the model of Padawer and Beecher, as it also considers the effect of the interaction of adjacent flakes. The fourth model, further improved for ordered nacre structure, is the shear tension model described by Kotha el Al [21] and adapted by Barthelat [30]. This "Shear Tension Model" considers the gap distance between tablets, the overlap ratio, and several geometrical variables and material property variables. Several assumptions are necessary to consider the model accurate. For this work, not all assumptions are valid, which is discussed further in the model section of this paper. Another model for the tablet–matrix composite was developed by Sakhvan et al. [31–33], to be a universal map for nacre-like structure design. However, with similar assumption requirements as the previous model, it has limited accuracy for the prediction of hexagonal-based tablet structures. We present a model that is suitable for hexagonal-shaped tablets inspired from the work of Barthelat [30] with the use of stiffness of volumes in series, and the work of Bar-On and Wagner [34] and Jaeger and Fratzl [35] with the use of Voigt model to calculate the stiffness of partial volumes of a representative volume element (RVE). As previously presented models assume that gaps between tablets are negligible and do not accurately predict the stiffness of the structure, the model and method for experimental validation presented in this work could allow for the acceleration of the design and development of highly ordered hexagonal nacre-like structures.

Carbon foils referred to as nanocrystalline diamond foils have measured stiffness of 600 GPa with a 50 μm thickness, as presented by Lodes et al. [36]. If the laser-cutting method is used to produce carbon-based hexagonal connected tablet, it can be combined with epoxy matrix material with stiffness of 3 GPa and maximum strain of 8.3%, as measured in the work of Shi et al. [37]. The manufacturing process and combination method could produce a composite with exceptional stiffness, strength, and toughness.

2. Materials and Methods

Nacre is a combination of brittle high stiffness reinforcing component and a tough low-stiffness binder matrix. The soft matrix stiffness in natural nacre is three orders of magnitude lower than the ceramic stiffness, as stated by Kim et al. [38], but analytical and simulation work has been done with the interface to reinforcement stiffness ratio ranging between 10 and 0.001. Ni et al. [39] summarize several nacreous composites with reinforcement elastic modulus to matrix shear modulus ratio ranging from 27 to 3800. Stiffness combination is not enough to provide toughness; the matrix material must have a relatively high plastic strain so that the composite can absorb energy [30]. The almost incompressibility of the matrix (high Poisson's ratio) is favorable for increased stiffness and strength [40]. An additional requirement to obtain a high-strength composite is bonding strength and the shear strength of the matrix component. However, as the focus of this investigation is stiffness validation, the material selection did not take strength requirement as an essential criterion [41]. Among polymers, polystyrene has a very high brittleness with a brittleness index B [42,43], nine times larger than other polymers on average. The brittleness is calculated using Equation (1), where E′ is the storage modulus determined by dynamic mechanical analysis at 1 Hz and room temperature, and ε_b is the elongation at break.

$$B = 1/(\varepsilon_b E') \quad (1)$$

Polystyrene is available in sheet form of micron range thickness. Polystyrene can be cut-processed into shape with laser energy methods, without toxicity risks, and with relatively low energy values compared to laser cut glass [25].

Glass would not be a suitable candidate as it is challenging to process with laser and is energy-intensive. Glass is also difficult and expensive to obtain in thin sheet form [30,44]. The thinnest currently available glass sheet is called D263 at 0.03 mm (SCHOTT North America Inc., Duryea, PA, USA). Glass is also so brittle that several layers would be difficult to laminate by hand, and would tend to crack when applying pressure in order to squeeze the matrix thin between the layers. Other ceramics would also not be suitable for laser processing and costly to obtain as thin sheets.

Polystyrene sheets are available at 135 µm thickness (Evergreen Scale Models, Des Plaines, IL, USA). The sheets are perfectly transparent and with a mirror polish surface. They are cleaned in an ultrasonic bath then cut with a laser to the desired shape. Laser cutting involves high temperatures that cause thermal degradation of polymers. The molecular weight of polystyrene near the cut areas is expected to drop. However, the work of McCormick et al. [45] showed that the stiffness of polystyrene does not change considerably with a reduction in molecular weight. The cutting geometry is similar to the hexagonal shape of nacre but leaves small bridges connecting adjacent plates. Such bridges are also described in the work of Ghazlan et al. [46] but with a different purpose. The bridges in this work allow the tablets to stay in position when assembling the structure, while, in previous work, the bridges have considerably larger cross-section and are used to increase stiffness in the structure.

Polystyrene has an acceptable bond strength to polyurethane, as stated by Hall et al. [47]; it can be further enhanced through surface plasma treatment or surface sulfonation [48]. Polyurethane is available as a relatively low viscosity mixture with reaction times longer than ten minutes, which is enough time to make a composite assembly. Polyurethane has considerable plasticity and stiffness, which is expected to be five to ten times less than polystyrene. One additional advantage of this selected polyurethane is that the final solid form is translucent, which allows for microscopic imagining of the assembly and the detection of trapped air cavitation.

Polyurethane resin SK6812 with a hardener of code 7802 (S U. K Hock GmbH, Regen, Germany) is mixed in an equal weight ratio as recommended by the manufacturer to obtain the expected properties. Twelve minutes is the curing time during which the viscosity increases until the solution turns solid, and it is no longer possible to laminate polystyrene layers. The resin has a viscosity of 130–150 mPas, and the hardener has a viscosity of 70 to 80 mPas. According to the material data sheet of the manufacturer, cured material is expected to have an ultimate tensile strength of 23 MPa and a maximum strain of 20%, as well as a flexural modulus (assumed equal to tensile elastic-modulus) by three point-bending of 0.56 GPa and impact strength of 10 KJ/m^2 based on DIN 53457 and DIN 53454 respectively.

Before proceeding with the composite assemblies, each material is characterized mechanically. Polystyrene sheet samples are tested following standard DIN EN ISO 527-3:2019-02 – ASTM D882, resulting in tensile stiffness of 2.66 GPa along the extrusion direction of the sheets. A stiffness of 2.64 GPa is measured perpendicular to the extrusion direction. As the difference in stiffness is not large, the average stiffness of 2.65 ± 0.04 GPa can be assumed. A more significant difference is measured in the strength of the film, with 50.06 ± 3.7 MPa in the extrusion direction and 43.76 ± 1.6 MPa perpendicular to extrusion. Such a difference does not affect the stiffness measurement of the composite assembly. PU samples were cast in additively manufactured molds. The molds are made using PolyVinyl Alcohol (PVA) polymer filament, which can be dissolved in water. PU mix is cast in the dissolvable mold, left for seven days to cure, then dissolved in water to release the specimens, the specimens are then dried and tested following the standard (DIN EN ISO 527-2) which resulted in a stiffness value of 0.35 ± 0.02 GPa. Delamination tests are also conducted following the standard ASTM D3163 with PU bonded to PS sheets. The delamination tests resulted in a shear strength value of 0.39 MPa.

The tensile test data, including strain measurements obtained by digital image correlation (DIC) method, also allowed the calculation of the Poisson's ratios of PS and PU, which were, respectively, 0.35 and 0.41. A high Poisson ratio confirms higher incompressibility of PU. The software used for (DIC) is Istra4D (Dantec Dynamics A/S, Skovlunde, Denmark), which uses a full-field image analysis. Square quadratic elements of 15 pixels were used to divide the region of interest (ROI), which consists of 1936

× 1216 pixels. The ROI is divided into 10660 (130 × 82) quadratic elements. A displacement uncertainty of 0.4 µm was recorded for a displacement of 100 µm. With the same cameras and software used, the work of Hack et al. [49] reported a strain measurement error of less than 3% in-plane. Using the Poisson's ratio and stiffness value of PU, the shear modulus G can be calculated using Equation (2) [50], resulting in G = 0.124 GPa.

$$G = \frac{E}{2\,(1+\upsilon)} \tag{2}$$

The layers are laminated on a designed plate with alignment pins to ensure the best possible overlap between the tablets. Three specimens were produced by combining six alternative layers for each. The manufactured composite laminates are measured by digital microscope Olympus DXS500 (Olympus Deutschland GmbH, Hamburg, Germany) to determine matrix layer thickness, overlap, and alignment accuracy. The measurements were used to create an accurate CAD model of the assembly. The model is meshed with quadratic tetrahedral elements. Material properties of the bi-components are assigned to the model, and then periodic boundary conditions are used to simulate an infinite laminate of also infinite layers. The samples in the simulation are under a uniaxial strain of 1% in full elastic behavior. With a small strain value and elastic material behavior, the element size used was half of the smallest geometrical feature, which is the reinforcement thickness of 0.135 µm.

3. Results

3.1. Experimental

Thin polystyrene films of 135 µm thickness with a measured stiffness of 2.65 GPa and polyurethane liquid resin mixture with resulting stiffness measured to be 0.35 GPa are then combined composite materials to investigate nacre-like structure stiffness. The PS sheets are processed with a laser-cutting machine Rayjet 50 (Trotec Laser GmbH, Wels, Austria) to obtain the final geometry shown in Figure 1a. Several laser-cut tests are run to obtain the nacre geometry with minimal cut line width. The optimal cut settings are 1% power of a 30 Watts CO_2 laser head with two to four passes, which resulted in a cut width (kerf) of 280 µm. The generated cut sheet is shown in Figure 1b with final tablet width of 4.22 mm.

The cut nacre sheets are cleaned in an ultrasound water bath and then accurately assembled on an assembly board using the cut guide holes shown in Figure 1c to align the tablet overlap. At the end of the assembly, a deadweight is added above the laminates to apply 20 kPa pressure, so that the matrix layers flow and become thinner, while the polystyrene is not damaged. The assembled sheets are left for seven days to cure properly before releasing them from the assembly board. Three nacre-like specimens are produced and then tested in tensile load using a universal high-precision tensile-testing machine Shimadzu AGS-X (Shimadzu, Kyoto, Japan) at 0.5 mm/min displacement. The strain is measured using the DIC system with high precision cameras Limess Q400 (LIMESS Messtechnik u. Software GmbH, Krefeld, Germany). The measured stiffness values for three specimens are 1.221 ± 0.012 GPa. The specimens failed at a stress of 6.7 ± 0.3 MPa and a maximum strain of 0.217 ± 0.0134.

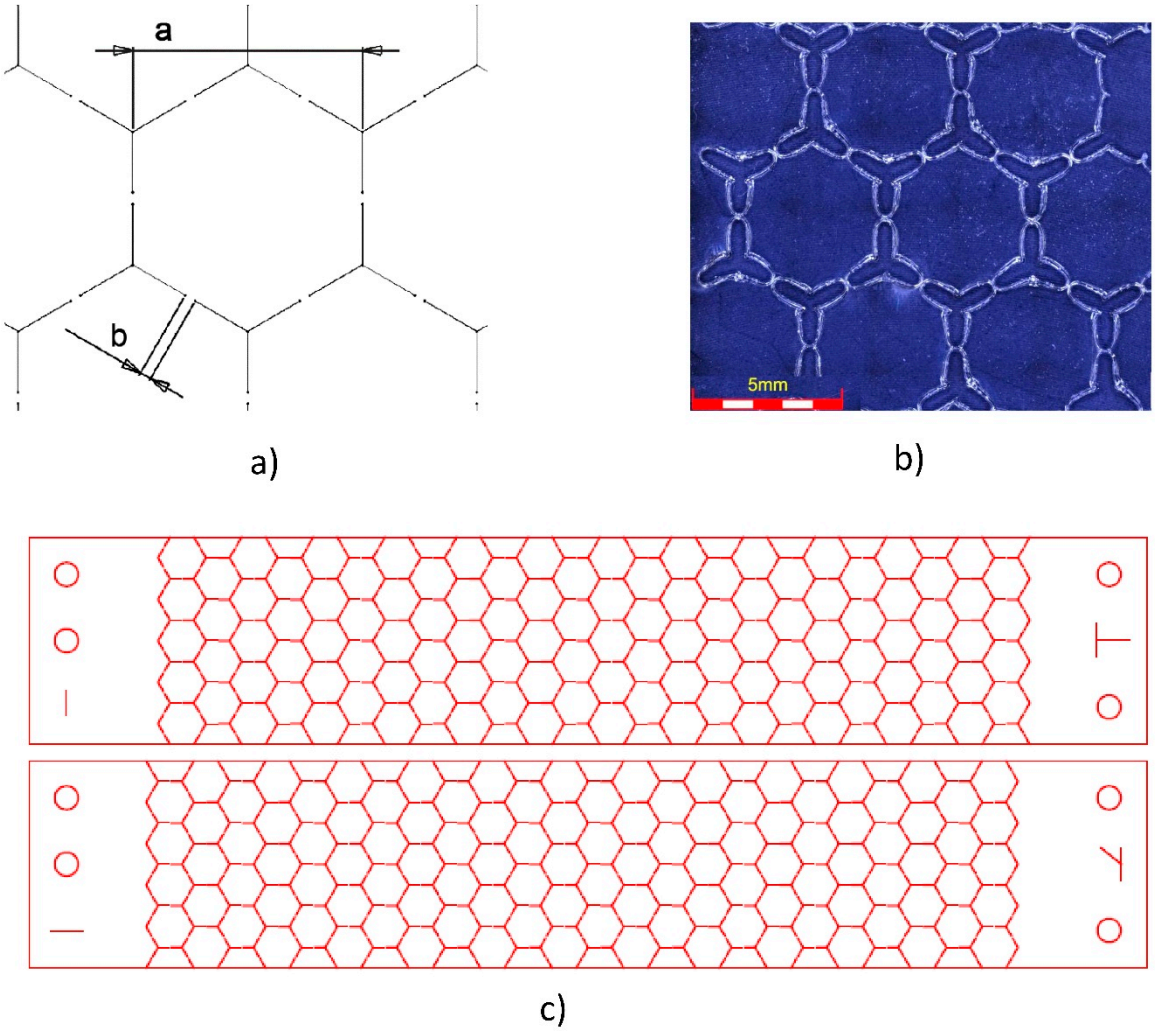

Figure 1. Polystyrene Laser cutting. (**a**) Designed cut lines (**b**) Laser cut view under a microscope (**c**) Laminate cut design with guide holes and orientation labels.

3.2. FEM

The manufactured experimental nacre laminates are measured with the Opto-digital microscope before being destroyed in the tensile tests. All measured features are modeled in CAD, and then the specimens are meshed in FEM software Simulia/Abaqus with a mesh size of 0.065 µm of quadratic tetrahedral elements. A smaller mesh element size was tested but resulted in no significant change in calculated stiffness. The materials are defined as linear elastic, with properties described in Table 1. The Poisson's ratios are calculated based on the strain values measured in the DIC of each composite component.

Table 1. Material mechanical properties.

Material	Stiffness (GPa)	Poisson's Ratio
Polystyrene	2.65	0.35
Polyurethane	0.35	0.41

The components of this FEM are partitioned from the same part, so that no interaction conditions where necessary, and thus debonding was not possible in the model. As the materials are linear, and the goal is to calculate composite stiffness, a total strain of 1% is applied to the representative volume element shown in Figure 2c. The measured hexagonal width was 4.22 mm, the side length was

2.442 mm, the cut gap was 280 µm, and the bridge width was 0.4 mm, shown in Figure 2a. Figure 2b shows the increase in the thickness of the polystyrene sheets due to the laser energy melting the polymer along the cut line. The increase in width that we refer to as a bulge has a total thickness of 250 µm and a width of 160 µm. The bulge is added to the CAD model of the RVE to represent the reinforcement tablets more accurately. Due to the bulge and limited pressure used when laminating the layers, the matrix layer thickness remained relatively large, with a value of 168 µm.

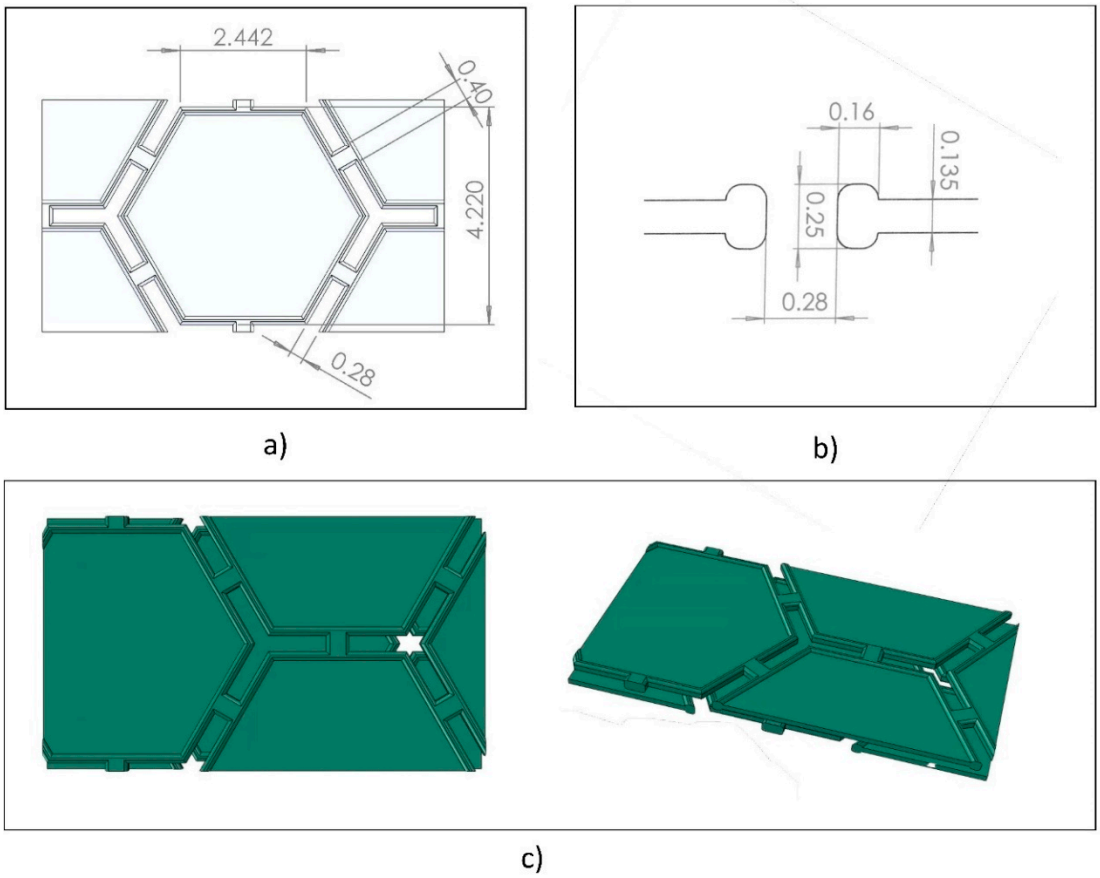

Figure 2. Measured and drawn geometry of the laminated polystyrene plates. (**a**) Tablet dimensions, (**b**) Bulge section view with dimensions. (**c**) Representative volume element (RVE) CAD model representing polystyrene cut tablets.

Periodic boundary conditions are used so that the stress calculations are, for an infinite repetitive body, in all three directions: X, Y, and Z. The resultant stiffness value was 1.21 GPa, which has a ~1% difference compared to the experimental value. It is important to note that a nacre RVE is not symmetric but only periodic, which makes some analytical models not suitable for a hexagonal-based tablet when compared to simplified rectangular tablets with half-length overlap. Periodic models such as RVE have been previously shown to more accurately estimate the composite structure stiffness than analytical models if they are correctly modeled [51]. This RVE of nacre is the minimum required volume to represent the composite, as the structure is periodic and very ordered, with known reinforcement dimensions and orientation governed by the lamination assembly process.

3.3. Analytical Stiffness

Once the experimental value and simulation value of stiffness was obtained, calculations were made using several analytical models to compare the analytical values and identify the error in every model.

3.3.1. Voigt Model

The Voigt model, represented by Equation (3), is used to calculate the axial loading stiffness of endless fiber composites [19]. It is generally known as the rule of mixture and is only dependent on the volume of the reinforcing material relative to the matrix material. This is the simplest model to make a prediction of stiffness, but as a nacre structure is not fiber-based with endless length, and has no specific orientation, this model cannot be considered as valid for nacre. Nevertheless, it is used to compare the nacre stiffness to a fiber composite of the same volume ratios and materials

$$E_c = f\, E_f + (1 - f)\, E_m \tag{3}$$

where E_f is the stiffness of the fibers, E_m is the stiffness of the matrix, and f is the volume fraction of fibers relative to total volume or, in this case, polystyrene hexagonal plates relative to polyurethane matrix. Based on the CAD model generated from microscope measured values, the volume of reinforcement element relative to total composite volume is 42.59%, which results in a stiffness of 1.33 GPa, which is 8.9% higher than the simulation value. Tablet composite stiffness is expected to approach the Voigt model when the length to thickness ratio exceeds 100 and tends to infinity [28,52]. With a ratio averaged at ~34 (4.55/0.135) for a hexagonal plate, this composite has a stiffness value lower than the Voigt model predicts.

3.3.2. Padawer and Beecher

Padawer and Beecher [28] made an early attempt to develop a predictive stiffness model for nacre-like structures. As the rule of mixture is only valid for continuous sheet, a model for discontinuous planar reinforcement was needed. Assuming that the reinforcing flakes have uniform width and uniform thickness, the aspect ratio α is the first variable used to estimate the stiffness of the flake-reinforced composites. Important assumptions are also necessary, as the reinforcing element needs to be uniformly spaced and aligned to the plane. Such conditions are only valid when the composite is accurately designed and built, which is the case for the PS/PU composite. Additional assumptions are necessary for strength prediction, which do not fall in the scope of this work.

The Padawer–Beecher model depends on a constant "u" which is itself dependent on geometry, and material properties are shown in Equation (4). G_M is the shear modulus of the matrix material, in this case, polyurethane. vf is the volume fraction of reinforcement and E_R is the stiffness modulus of reinforcing material, in this case, the polystyrene films.

$$u = \alpha\left[\frac{(G_M)(vf)}{(E_R)(1 - vf)}\right]^{1/2} \tag{4}$$

The model makes use of a term called Modulus Reduction Factor (MRF). It is used as a stiffness reduction constant dependent on "u", as shown in Equation (5).

$$\mathrm{MRF} = [1 - \frac{\tanh(u)}{u}], \tag{5}$$

The stiffness model equation is very similar to the rule of mixture model but with the added multiplication with the MRF value, as shown in Equation (6).

$$E_C = (E_R)(vf)(\mathrm{MRF}) + (E_M)(1 - vf), \tag{6}$$

As we have experimentally obtained all material properties required for the calculation and the flakes are designed to have the same constant width of 4.22 mm and thickness of 135 µm, we can use the model and calculate a stiffness of 1.15 GPa where the MRF value is 0.841. It is important to note

that a higher flake volume ratio leads to an increase in MRF, and thus stiffness, but the increase is not significant above $\alpha = 100$, as explained by Padawer and Beecher [28].

3.3.3. Lusis et al.

The model developed by Padawer and Beecher does not take into consideration the interaction between the adjacent flakes. An adjustment was presented by Lusis et al. [29], with the MRF calculated following a logarithmic equation shown in Equation (7).

$$\mathrm{MRF} = [1 - \frac{\ln(u+1)}{\mathrm{u}}], \tag{7}$$

With this adjustment, the MRF value is expected to be lower, and thus the calculated material stiffness is 0.973 GPa. Based on the paper by Jackson et al. [52], generally, the prediction by Lusis tends to fall lower than experimental values, which is also the case in this work.

3.3.4. Shear Tension Model

The shear tension model is first described by Kotha et al. [21], and then adapted by Barthelat [30], like in most analytical models; there are important assumptions to make so that the model is considered valid. Kotha et al. [21] made four assumptions. The first is that the tablets are of uniform width, rectangular shape, and isotropic. The geometry of the tablets in the experimental work is hexagonal but has a defined width, and the material is quasi-isotropic, with little variation in stiffness with the change of direction. There is less than 0.7% difference in stiffness for PS along extrusion relative to lateral. In the second assumption, the tablets need to be uniformly arranged, which is valid in this work. With an overlap close to 30% and tablets accurately positioned, we can assume that the majority of the stresses are transferred from tablet to tablet by shear, which is the third assumption required. With the matrix having a low stiffness compared to the reinforcement, the fourth assumption is also valid, and the end of the tablets contribute little to stress transfer.

The model is dependent on several parameters shown in Table 2 with the relative equations to calculate the respective values of which volume fraction, aspect ratio for the tables, aspect ratio of tablet length to thickness and overlap ratio of tablet length. For a composite system dependent on shear transfer of stress, an elastic shear transfer number β_0 is derived and used to estimate the composite stiffness. It is important to note that the volume fraction value ϕ is dependent on tablet and interface thickness and assumes gaps between tablets to be negligible.

Table 2. Shear lag model equations and variables.

Parameter	Equation	Variables
Volume fraction	$\phi = \frac{t_t}{t_t + t_i}$	t_t tablet thickness t_i interface thickness
Aspect ratio of overlap region	$\rho_0 = \frac{L_0}{t_t}$	L_0 overlap length t_t tablet thickness
Overlap ratio	$k = \frac{L_0}{L}$	L tablet length $0 < k \leq 0.5$
Elastic shear transfer number	$\beta_0 = \rho_0 \sqrt{\frac{G_i}{E_t}\frac{t_t}{t_i}}$	G_i matrix shear modulus E_t tablet stiffness modulus
Non-Symmetric RVE Composite stiffness	$E = \frac{\phi E_t}{1 + \frac{k}{\beta_0}[\coth(\beta_0) + \coth(\frac{1-k}{k}\beta_0)]}$	-

The hexagonal tablet overlap has symmetry, as shown in Figure 3, which can be used to calculate the required variables. If the gaps between hexagons are neglected, we should obtain a stiffer model. Due to a non-rectangular geometry, half a hexagon with an edge length "a" of 2.44 mm, and a half area of 7.72 mm^2 with a half-width of 2.115 mm, can be approximated to a rectangle of 3.656 mm length.

Thus, an area overlap of 0.29% would be equivalent to an overlap length of 1.0627 mm. The volume fraction ϕ would be 0.4455 and the aspect ratio of the overlap region would be 7.87. The resultant shear transfer number would be β_0 = 1.527. The calculated stiffness with the simplified model is 0.845 GPa, which is considerably lower than the value calculated by the Lusis model [29].

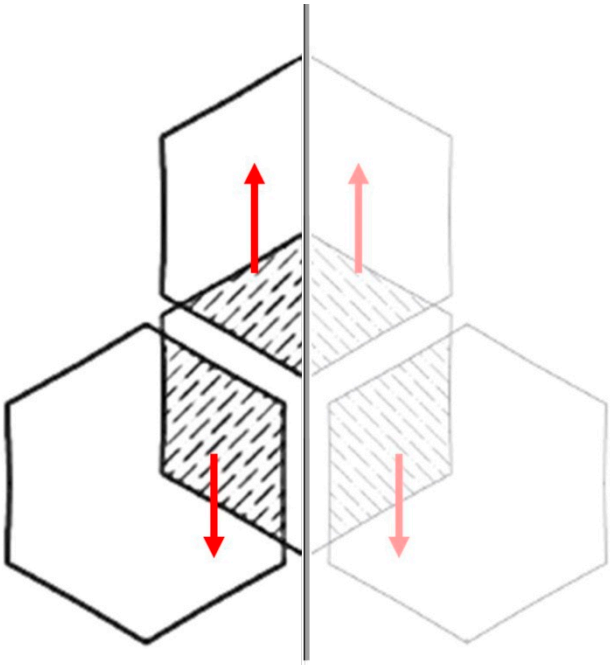

Figure 3. Volume symmetry of hexagonal reinforcement.

3.3.5. The Proposed Model for Highly Ordered Hexagonal Tablets

Using the well-defined geometry of the hexagonal tablets and assuming the complete linear elastic behavior of the material, we can simplify the composite representative volume as a rectangle divided into several zones of either one layer of reinforcement or two layers of reinforcement. Using the rule of mixture for every continuous and homogeneous area of overlap, we can calculate the stiffness of the areas. What other models do not take into consideration is the size of the gap between tablets, which is calculated in this model. Another assumption for the shear-lag model [30] is that the end of the tablets does not contribute to the stiffness of the model. This is taken into consideration in this model.

The RVE geometry of hexagonal nacre-like composite can be simplified, as in the half hexagonal volume shown in Figure 3; however, to be able to calculate using homogeneous volumes, the RVE is divided into several zones of known stiffness, shown in Figure 4.

Known parameters that are required would be, most importantly, the stiffness of the materials, the thickness of the reinforcing tablets, and matrix layers between them. In this specific case of hexagonal tablets, it is important to know at least one defining dimension of the hexagon, which is the short diagonal (The width of a hexagon). From the short diagonal "d", all other dimensions of a hexagon can be calculated. The edge length "a" is calculated by dividing the short diagonal by $\sqrt{3}$. Another important feature that is also relevant to the manufacturing method of these connected tablets would be the width of cut "c" (kerf). The width of the cut dictates the gap dimensions between the tablets in the same layers.

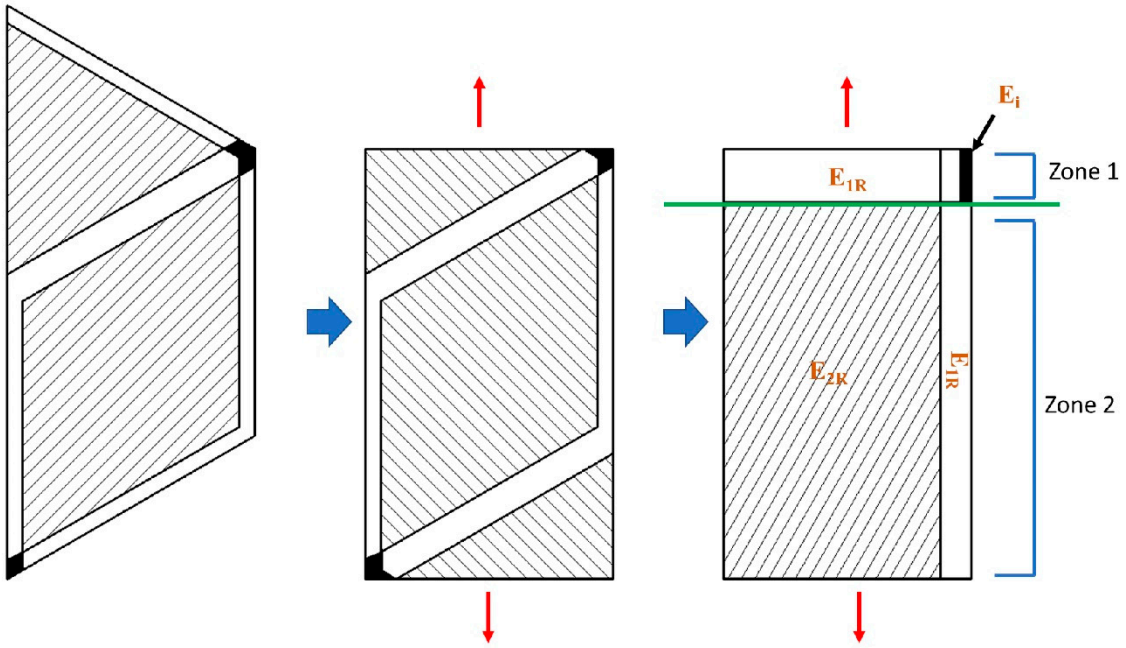

Figure 4. Volume simplification of hexagonal reinforcement.

The rectangular volume shown in Figure 4 would have a width W_r of half the short diagonal d_1. The rectangular length L_r is 1.5 times the edge length a. The double reinforced zone has a width $W_{1,}$ which is equal to the width of the rectangle without a kerf c width. The height of the double reinforcement zone (hatch-filled zone) is the length of the rectangle with two projected cut width removed L_r−2c/cos30. The height of the single-layer reinforcement (zone 1) is the width of two cuts projected at 30-degree angle 2c/cos30. The remaining zone highlighted in black is a non-reinforced area that can also be seen in Figure 2c; it has an equal area to a hexagon with short diagonal equal to the cut width c. The non-reinforced zone has a width of 0.375c and the same height of Zone 1.

In Figure 4, there are zones of a single layer of reinforcement with a stiffness we shall call E_{1R}. The remaining zones are of double layers of reinforcement with a stiffness we shall call E_{2R}. These stiffness values are calculated following the equations shown in Table 3, where t_t is the tablet thickness, t_i is the interface thickness, E_p is the tablet stiffness, and E_i is the interface stiffness.

Table 3. Hexagonal Composite Stiffness Model.

Parameter	Equation	Variables
Single reinforcing layer zone stiffness	$E_{1R} = \frac{t_t E_t + (t_t + 2t_i) E_i}{2(t_t + t_i)}$	t_t tablet thickness t_i Interface thickness
Double reinforcing layer zone stiffness	$E_{2R} = \frac{t_t E_t + t_i E_i}{t_t + t_i}$	E_t Tablet stiffness modulus E_i interface stiffness modulus
Hybrid zone stiffness 1	$E_{Hyb1} = \frac{0.75c}{d} E_i + \frac{d-0.75c}{d} E_{1R}$	-
Hybrid zone stiffness 2	$E_{Hyb2} = \frac{2c}{d} E_{1R} + \frac{d-2c}{d} E_{2R}$	c cut width d short diagonal
Stiffness ratio 1	$r_1 = \frac{2c}{L \cos 30 \, E_{Hyb1}}$	a edge length L = 1.5a rectangle height
Stiffness ratio 2	$r_2 = \frac{1}{E_{Hyb2}} - \frac{2c}{L \, cos30 \, E_{Hyb2}}$	-
Hexagonal Composite stiffness	$E_c = \frac{1}{r_1 + r_2}$	-

Along the load axis, the stiffness of Zone 1 is calculated following the Voigt model, with a dependence on width similar to the work of Jäger and Fratzl [35], resulting in hybrid zone stiffness

E_{Hyb1}. The stiffness of Zone 2 is calculated similarly, resulting in hybrid zone stiffness E_{Hyb2}. To calculate resultant composite stiffness of Zone 1 and Zone 2, the equation for zones acting in series is used, as suggested by Barthelat [30].

With the dimensions produced experimentally known, and the material properties measured, we can calculate E_{1R} to be 0.862 GPa, E_{2R} is 1.375 GPa, E_{Hyb1} is 0.838 and E_{Hyb2} is 1.358 GPa. The stiffness ratio values are as follows: r_1 is 0.198 GPa^{-1}, r_2 is 0.614 GPa^{-1}, resulting with a composite stiffness of 1.231 GPa.

The same method can be used with volume simplification to calculate stiffness for rectangular tablets with cut width and perfect positioning. The resulting equations are similar to the hexagonal equations but with cos30 angle projection removed, and the unreinforced, black-colored zone in Figure 4 has a width of c/2 in a rectangular composite when compared to a hexagonal composite with a non-reinforced zone of width 0.75c. The equations for rectangular tablet composite with cut width are shown in Table 4, with w being the rectangle width and L being the rectangle height. The advantage of hexagonal tablets remains, with quasi-isotropic stiffness in the plane.

Table 4. Rectangular Composite Stiffness Model.

Parameter	Equation	Variables
Single reinforcing layer zone stiffness	$E_{1R} = \frac{t_t E_t + (t_t + 2t_i) E_i}{2(t_t + t_i)}$	t_t tablet thickness t_i Interface thickness
Double reinforcing layer zone stiffness	$E_{2R} = \frac{t_t E_t + t_i E_i}{t_t + t_i}$	E_t Tablet stiffness modulus E_i interface stiffness modulus
Hybrid zone stiffness 1	$E_{Hyb1} = \frac{0.5c}{d} E_i + \frac{d-0.5c}{d} E_{1R}$	-
Hybrid zone stiffness 2	$E_{Hyb2} = \frac{2c}{d} E_{1R} + \frac{d-2c}{d} E_{2R}$	c cut width d rectangle width
Stiffness ratio 1	$r_1 = \frac{2c}{L E_{Hyb1}}$	L rectangle height
Stiffness ratio 2	$r_2 = \frac{1}{E_{Hyb2}} - \frac{2c}{L E_{Hyb2}}$	-
Hexagonal Composite stiffness	$E_c = \frac{1}{r_1 + r_2}$	-

4. Discussion

The calculated, simulated, and measured stiffness values are summarized in Table 5, with the percentage difference relative to the experimental value. The simulated value has a difference of 1% relative to the experimental value. The small difference can be explained by an accurate representation of the geometry by optical measurements and the accurate material characterization data used in the FEM model. However, the FEM is a long process and cannot allow quick iterations in design unless a parametric model is developed for specifically hexagonal tablets connected by thin bridges. The rule of mixture results in a considerably higher value because it assumes a continuous reinforcement with constant cross-section. At the same time, a hexagonal nacre-like structure is discontinuous and has a varying reinforcement cross-section, which leads to stiffness reduction. However, tablet-reinforced structures converge to the rule of mixture, as the aspect ratio tends towards infinity, as stated by Jackson et al. [52] and Bekah et al. [53]. In the case of the "Padawer & Beecher" and "Lusis" models, they both predict a lower stiffness than what is measured. This could be due to the shear modulus of the matrix material and the thickness of the interface layer. Jackson et al. [52] have shown that the value of shear modulus influences the prediction error in both models relative to the experimental. The model's accuracy is highly dependent on the interface layer thickness and mechanical properties, as it assumes that all loads are conveyed by shear stresses and ignores stresses in tension between the tablets. However, it is important to note that both models are developed for single-lap joint rectangular flakes [29].

Table 5. Stiffness of PS-PU Hexagonal Nacre-like Composite.

Method	Stiffness (GPa)	Difference from Experimental
Experimental	1.221	0%
Finite Element Method (FEM)	1.21	−1%
Rule of Mixture (Voigt Model)	1.33	+9%
Padawer and Beecher Model	1.15	−6%
Lusis et al. Model	0.973	−20%
Shear-lag Model	0.845	−31%
Hexagonal Model	1.231	+0.8%

Calculating following the shear lag model presented by Bathelat [30] resulted in the most significant difference of 31% from the measured value. While it was necessary to make important assumptions and approximations from hexagonal geometry to rectangular, and the model neglects any loads being conveyed between the tablets except by shear. The model assumes the spacing between the tablets to be negligible. In this example, the spacing is 6% of the tablet width. The model again appears to diverge from experimental results when the interface layer is comparable to the reinforcement layer in thickness. The hexagonal model presented here is derived from the exact geometry of the hexagonal nacre-like composite, assuming perfect positioning and consistent cut width. A 0.8% difference from the experimental value is as good as the FEM result. As the model is strictly dependent on material property, hexagon size, cut width, and reinforcement and interface thickness, it is easier to run fast iterations to identify more efficient composites with higher stiffness. It is also easy to predict the influence of important variables on the resultant stiffness, as shown in Figure 5. The matrix thickness reduces the stiffness of the hexagonal composite strongly as it nears the reinforcement tablet thickness, and as it becomes thicker, the stiffness no longer drops sharply. As shown in Figure 5a, with a matrix thickness of 0 mm, the maximum stiffness would be 2.392 GPa, which is 10% lower than the stiffness of the reinforcing material (while the cut width remains 0.28 mm), which indicates a considerable reduction of stiffness due to cut width. The PS-PU stiffness, with an interface of thickness 0.168 mm, in this case, is 52% of the maximum possible stiffness. Above a tablet width that is a hundred times the thickness (aspect ratio 100), the stiffness tends to the value calculated by the rule of mixture. With the PS-PU samples produced having a width to thickness ratio of 33, the stiffness is 91% of the rule of mixture value, as shown in Figure 5b. While maintaining an interface thickness of 0.168 mm and Hexagonal dimension, the reduction in cut width tends to increase the stiffness closer to the rule of mixture value without changing the tablet aspect ratio. Again, the PS-PU composite has a stiffness that is 91% of the rule of mixture value, as shown in Figure 5c. Thus, we could summarize that the reduction in matrix layer thickness could yield the highest stiffness value, close to the reinforcing material stiffness. Cut width reduction and hexagonal size increase brings the stiffness value closer to what the rule of mixture suggests.

In Figure 5a, the plotted stiffness calculated by the Padawer and Beecher model is consistently lower than the simulation and experimental work. If cut width is considered negligible in the model, thus adjusting aspect ratio and reinforcement volume, the plotted stiffness curve referred to with "NC" (no cut width) is brought closer to simulation values. The hexagonal model is closest to simulation values. Figure 5b shows both Padawer and Beecher models mentioned and the Hexagonal model Ec. The adjusted Padawer and Beecher model (NC) is brought closer to simulated values and is more accurate when the tablets are smaller relative to the gaps. The significant advantage of the Hexagonal Model is shown in Figure 5c, where the Ec plot aligns better with simulated values when the Kerf increases.

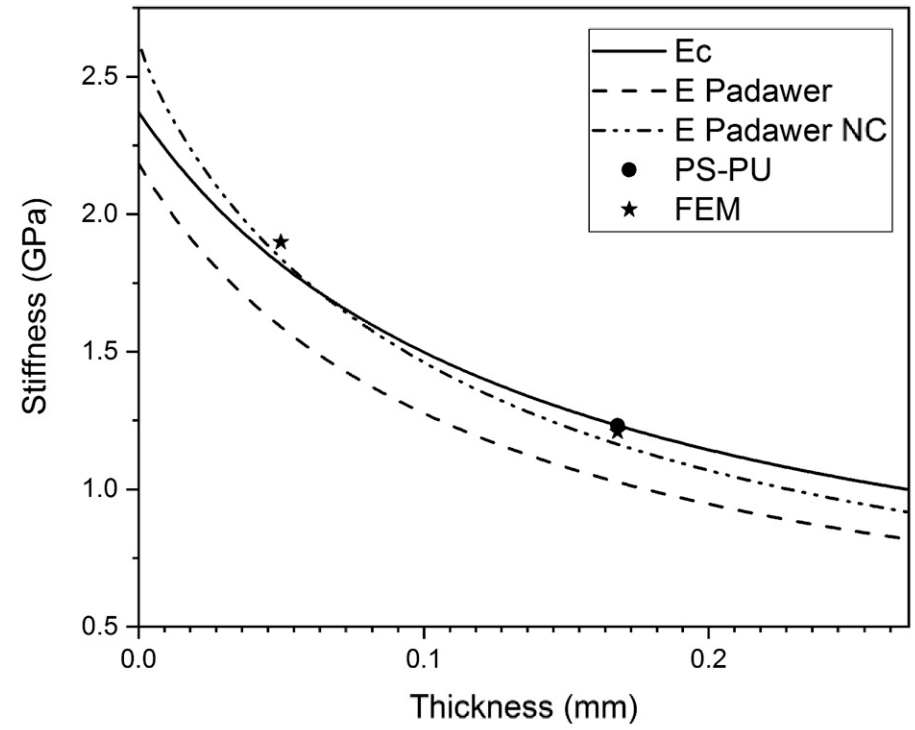

a)

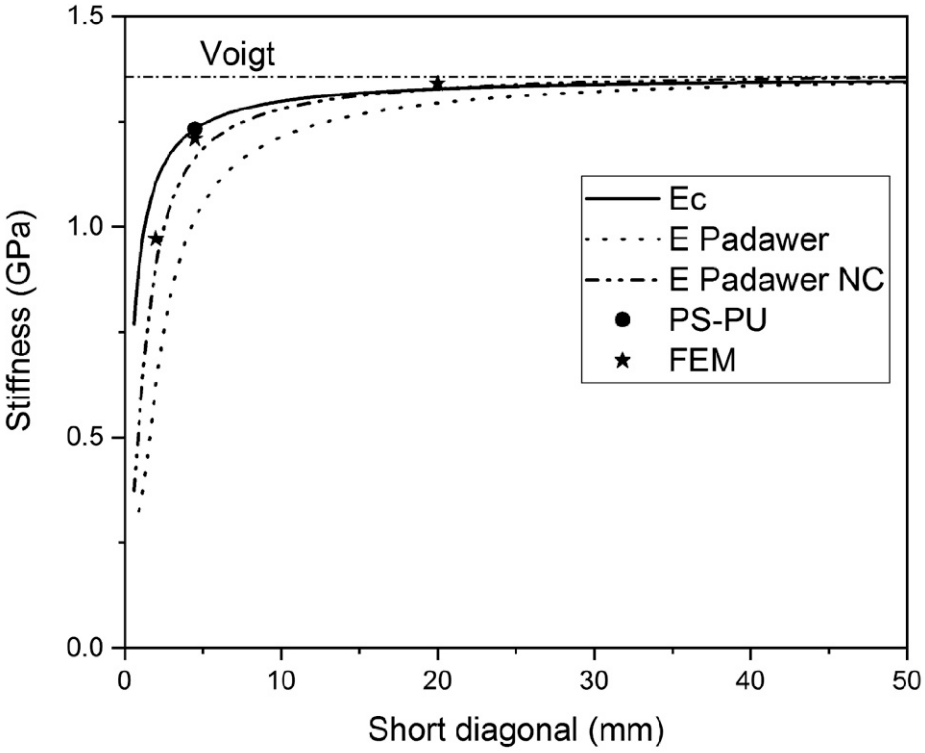

b)

Figure 5. *Cont.*

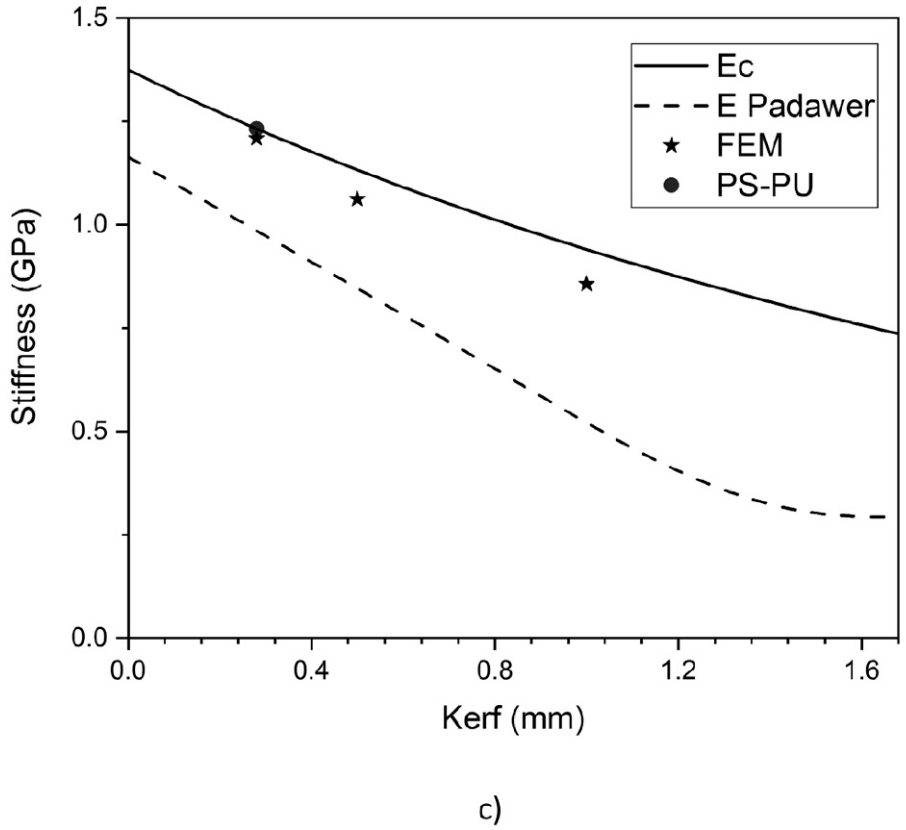

Figure 5. Processing influence on hexagonal composite stiffness, (**a**) Matrix thickness, (**b**) Hexagonal short diagonal, (**c**) cut width.

5. Example

As polystyrene is not the right candidate for high strength composites and is only used for experimental validation of the model, a carbon film with epoxy matrix composite has its stiffness predicted using the hexagonal model using the carbon films described earlier with a stiffness of 600 GPa and a thickness of 50 µm [36] and epoxy resins matrix of stiffness 3 GPa [37], assuming that interface thickness is equal to reinforcing layer thickness and the cut width is 35 µm, based on the laser cut notches using YAG solid-state laser as described by Lodes et al. [36]. The determined values can then be used to plot the change in composite stiffness depending on the size of the hexagonal tablet shown in Figure 6.

With a hexagon diagonal width of 1.53 mm, the stiffness of the composite is at 95% of the Voigt model stiffness value. Increasing the hexagonal width to 5.25 mm brings the stiffness to 99% of the Voigt model. The size of the hexagon, in this case, should also be connected to the energy spent to do the cutting, as smaller hexagons require more cutting travel perimeter in a unit area. For later development, the hexagonal size must be optimized to minimize energy, maintain stiffness and strength, and maximize toughness.

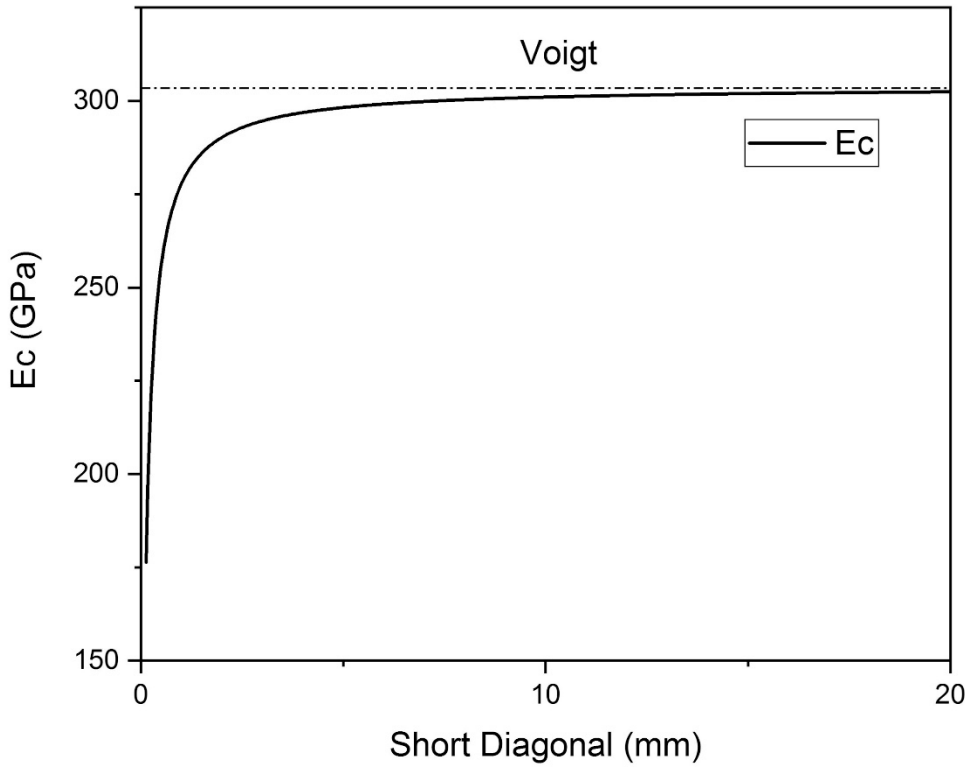

Figure 6. Carbon-Epoxy hexagonal composite stiffness.

6. Conclusions

The hexagonal stiffness prediction model could allow fast design iterations for hexagonal nacre-like composites. The resultant geometry can then be validated using the experimental method described using polystyrene thin film and polyurethane as a matrix material. The FEM simulation method would serve as an additional validation method for the design. It is important to note that the presented manufacturing methods of a hexagonal nacre-like composite results in unavoidable cut width from an endless sheet of reinforcing material. Such a cut width can be reduced depending on the cutting method used and can be optimized for each method. In the example of laser cutting, the process involves parameters such as laser power and cutting speed. The thickness of the reinforcing tablets depends on the material selected and the method used to produce the material film. The original film thickness is the base dimension on which a hexagonal composite can be designed. It leads to the selection of hexagonal size to maintain an optimal aspect ratio for maximizing stiffness.

For practical and industrial applications, the Hexagonal Model could be used to predict the stiffness of mass-produced composites, using cutting methods and with controlled interface thickness. As the mechanical performance of a composite is also dependent on strength and toughness, specific prediction models are still required for those properties, and this stiffness model could serve as a guide.

Author Contributions: Conceptualization, R.R.; methodology, R.R.; software, M.S.; validation, M.S., and R.R.; formal analysis, R.R.; investigation, R.R.; resources, M.S.; data curation, R.R.; writing—original draft preparation, R.R.; writing—review and editing, R.R.; visualization, R.R.; supervision, M.S.; project administration, R.R.; funding acquisition, M.S. All authors have read and agreed to the published version of the manuscript.

Funding: This research received no external funding.

Acknowledgments: The authors would like to Thank Kevin Breuer and Patrick Gahlen for providing the python script to run the FEM simulations. The authors acknowledge the financial support by the German Research Foundation (DFG)and TU Dortmund University within the funding program "Open Access Publishing".

Conflicts of Interest: The authors declare no conflict of interest.

References

1. Bouville, F. Strong and tough nacre-like aluminas: Process–structure–performance relationships and position within the nacre-inspired composite landscape. *J. Mater. Res.* **2020**, *9*, 1–19. [CrossRef]
2. Al-Maskari, N.S.; McAdams, D.A.; Reddy, J.N. Modeling of a biological material nacre: Waviness stiffness model. *Mater. Sci. Eng. C Mater. Biol. Appl.* **2017**, *70*, 772–776. [CrossRef] [PubMed]
3. Barthelat, F.; Yin, Z.; Buehler, M.J. Structure and mechanics of interfaces in biological materials. *Nat. Rev. Mater.* **2016**, *1*, 1144. [CrossRef]
4. Wang, R.Z.; Suo, Z.; Evans, A.G.; Yao, N.; Aksay, I.A. Deformation mechanisms in nacre. *J. Mater. Res.* **2001**, *16*, 2485–2493. [CrossRef]
5. Currey, J.D. Mechanical properties of mother of pearl in tension. *Proc. R. Soc. Lond. B* **1977**, *196*, 443–463. [CrossRef]
6. Budarapu, P.R.; Thakur, S.; Kumar, S.; Paggi, M. Micromechanics of engineered interphases in nacre-like composite structures. *Mech. Adv. Mater. Struct.* **2020**, *6*, 1–16. [CrossRef]
7. Yin, Z.; Hannard, F.; Barthelat, F. Impact-resistant nacre-like transparent materials. *Science* **2019**, *364*, 1260–1263. [CrossRef]
8. Valashani, S.M.M.; Barthelat, F. A laser-engraved glass duplicating the structure, mechanics and performance of natural nacre. *Bioinspir. Biomim.* **2015**, *10*, 26005. [CrossRef]
9. Narducci, F.; Pinho, S.T. Exploiting nacre-inspired crack deflection mechanisms in CFRP via micro-structural design. *Compos. Sci. Technol.* **2017**, *153*, 178–189. [CrossRef]
10. Grossman, M.; Pivovarov, D.; Bouville, F.; Dransfeld, C.; Masania, K.; Studart, A.R. Hierarchical Toughening of Nacre-Like Composites. *Adv. Funct. Mater.* **2019**, *29*, 1806800. [CrossRef]
11. Launey, M.E.; Munch, E.; Alsem, D.H.; Saiz, E.; Tomsia, A.P.; Ritchie, R.O. A novel biomimetic approach to the design of high-performance ceramic-metal composites. *J. R. Soc. Interface* **2010**, *7*, 741–753. [CrossRef] [PubMed]
12. Muñoz, M.; Cerbelaud, M.; Videcoq, A.; Saad, H.; Boulle, A.; Meille, S.; Deville, S.; Rossignol, F. Nacre-like Alumina Composites Based on Heteroaggregation. *J. Eur. Ceram. Soc.* **2020**. [CrossRef]
13. de Luca, F.; Sernicola, G.; Shaffer, M.S.P.; Bismarck, A. "Brick-and-Mortar" Nanostructured Interphase for Glass-Fiber-Reinforced Polymer Composites. *ACS Appl. Mater. Interfaces* **2018**, *10*, 7352–7361. [CrossRef] [PubMed]
14. Mirkhalaf, M.; Zreiqat, H. Fabrication and Mechanics of Bioinspired Materials with Dense Architectures: Current Status and Future Perspectives. *JOM* **2020**, 1458–1476. [CrossRef]
15. Wegst, U.G.K.; Bai, H.; Saiz, E.; Tomsia, A.P.; Ritchie, R.O. Bioinspired structural materials. *Nat. Mater.* **2015**, *14*, 23–36. [CrossRef]
16. Grujicic, M.; Ramaswami, S.; Snipes, J. Nacre-like ceramic/polymer laminated composite for use in body-armor applications. *AIMS Mater. Sci.* **2016**, *3*, 83–113. [CrossRef]
17. Raj, M.; Patil, S.P.; Markert, B. Mechanical Properties of Nacre-Like Composites: A Bottom-Up Approach. *J. Compos. Sci.* **2020**, *4*, 35. [CrossRef]
18. Liu, F.; Li, T.; Jia, Z.; Wang, L. Combination of stiffness, strength, and toughness in 3D printed interlocking nacre-like composites. *Extrem. Mech. Lett.* **2020**, *35*. [CrossRef]
19. Voigt, W. Ueber die Beziehung zwischen den beiden Elasticitätsconstanten isotroper Körper. *Ann. Phys.* **1889**, *274*, 573–587. [CrossRef]
20. Kim, Y.; Kim, Y.; Libonati, F.; Ryu, S. Designing tough isotropic structural composite using computation, 3D printing and testing. *Compos. Part B Eng.* **2019**, *167*, 736–745. [CrossRef]
21. Kotha, S.P.; Li, Y.; Guzelsu, N. Micromechanical model of nacre tested in tension. *J. Mater. Sci.* **2001**, 2001–2007. [CrossRef]
22. Liu, G.; Ji, B.; Hwang, K.-C.; Khoo, B.C. Analytical solutions of the displacement and stress fields of the nanocomposite structure of biological materials. *Compos. Sci. Technol.* **2011**, *71*, 1190–1195. [CrossRef]
23. Bonderer, L.J.; Chen, P.W.; Kocher, P.; Gauckler, L.J. Free-Standing Ultrathin Ceramic Foils. *J. Am. Ceram. Soc.* **2010**, *93*, 3624–3631. [CrossRef]
24. Miao, T.; Shen, L.; Xu, Q.; Flores-Johnson, E.A.; Zhang, J.; Lu, G. Ballistic performance of bioinspired nacre-like aluminium composite plates. *Compos. Part B Eng.* **2019**, *177*, 107382. [CrossRef]

25. Mirkhalaf, M.; Dastjerdi, A.K.; Barthelat, F. Overcoming the brittleness of glass through bio-inspiration and micro-architecture. *Nat. Commun.* **2014**, *5*, 3166. [CrossRef] [PubMed]
26. Luz, G.M.; Mano, J.F. Biomimetic design of materials and biomaterials inspired by the structure of nacre. *Philos. Trans. A Math. Phys. Eng. Sci.* **2009**, *367*, 1587–1605. [CrossRef]
27. *Abaqus 2017*; Dassault Systèmes Simulia: Vélizy-Villacoublay, France, 2020.
28. Padawer, G.E.; Beecher, N. On the strength and stiffness of planar reinforced plastic resins. *Polym. Eng. Sci.* **1970**, *10*, 185–192. [CrossRef]
29. Lusis, J.; Woodhams, R.T.; Xanthos, M. The effect of flake aspect ratio on the flexural properties of mica reinforced plastics. *Polym. Eng. Sci.* **1973**, *13*, 139–145. [CrossRef]
30. Barthelat, F. Designing nacre-like materials for simultaneous stiffness, strength and toughness: Optimum materials, composition, microstructure and size. *J. Mech. Phys. Solids* **2014**, *73*, 22–37. [CrossRef]
31. Sakhavand, N. Mechanics of Platelet-Matrix Composites across Scales: Theory, Multiscale Modeling, and 3D Fabrication. *Mater. Sci.* **2015**, *79–05*, 292.
32. Sakhavand, N.; Muthuramalingam, P.; Shahsavari, R. Toughness governs the rupture of the interfacial H-bond assemblies at a critical length scale in hybrid materials. *Langmuir* **2013**, *29*, 8154–8163. [CrossRef] [PubMed]
33. Sakhavand, N.; Shahsavari, R. Universal composition-structure-property maps for natural and biomimetic platelet-matrix composites and stacked heterostructures. *Nat. Commun.* **2015**, *6*, 6523. [CrossRef] [PubMed]
34. Bar-On, B.; Wagner, H.D. New insights into the Young's modulus of staggered biological composites. *Mater. Sci. Eng. C Mater. Biol. Appl.* **2013**, *33*, 603–607. [CrossRef] [PubMed]
35. Jäger, I.; Fratzl, P. Mineralized Collagen Fibrils: A Mechanical Model with a Staggered Arrangement of Mineral Particles. *Biophys. J.* **2000**, *79*, 1737–1746. [CrossRef]
36. Lodes, M.A.; Kachold, F.S.; Rosiwal, S.M. Mechanical properties of micro- and nanocrystalline diamond foils. *Philos. Trans. A Math. Phys. Eng. Sci.* **2015**, *373*. [CrossRef]
37. Shi, H.-Q.; Sun, B.-G.; Liu, Q.; Yang, Z.-Y.; Yi, K.; Zhang, Y.; Fu, S.-Y. A high ductility RTM epoxy resin with relatively high modulus and Tg. *J. Polym. Res.* **2015**, *22*, 435. [CrossRef]
38. Kim, Y.; Kim, Y.; Lee, T.-I.; Kim, T.-S.; Ryu, S. An extended analytic model for the elastic properties of platelet-staggered composites and its application to 3D printed structures. *Compos. Struct.* **2018**, *189*, 27–36. [CrossRef]
39. Ni, Y.; Song, Z.; Jiang, H.; Yu, S.-H.; He, L. Optimization design of strong and tough nacreous nanocomposites through tuning characteristic lengths. *J. Mech. Phys. Solids* **2015**, *81*, 41–57. [CrossRef]
40. Tushtev, K.; Murck, M.; Grathwohl, G. On the nature of the stiffness of nacre. *Mater. Sci. Eng. C* **2008**, *28*, 1164–1172. [CrossRef]
41. Wei, X.; Naraghi, M.; Espinosa, H.D. Optimal length scales emerging from shear load transfer in natural materials: Application to carbon-based nanocomposite design. *ACS Nano* **2012**, *6*, 2333–2344. [CrossRef]
42. Brostow, W.; Hagg Lobland, H.E.; Narkis, M. Sliding wear, viscoelasticity, and brittleness of polymers. *J. Mater. Res.* **2006**, *21*, 2422–2428. [CrossRef]
43. Brostow, W.; Hagg Lobland, H.E.; Khoja, S. Brittleness and toughness of polymers and other materials. *Mater. Lett.* **2015**, *159*, 478–480. [CrossRef]
44. Chintapalli, R.K.; Breton, S.; Dastjerdi, A.K.; Barthelat, F. Strain rate hardening: A hidden but critical mechanism for biological composites? *Acta Biomater.* **2014**, *10*, 5064–5073. [CrossRef] [PubMed]
45. McCormick, H.W.; Brower, F.M.; Kin, L. The effect of molecular weight distribution on the physical properties of polystyrene. *J. Polym. Sci.* **1959**, *39*, 87–100. [CrossRef]
46. Ghazlan, A.; Ngo, T.; van Le, T.; Nguyen, T.; Remennikov, A. Blast performance of a bio-mimetic panel based on the structure of nacre—A numerical study. *Compos. Struct.* **2020**, *234*, 111691. [CrossRef]
47. Hall, J.R.; Westerdahl, C.A.L.; Devine, A.T.; Bodnar, M.J. Activated gas plasma surface treatment of polymers for adhesive bonding. *J. Appl. Polym. Sci.* **1969**, *13*, 2085–2096. [CrossRef]
48. Erickson, B.L.; Asthana, H.; Drzal, L.T. Sulfonation of polymer surfaces—I. Improving adhesion of polypropylene and polystyrene to epoxy adhesives via gas phase sulfonation. *J. Adhes. Sci. Technol.* **1997**, *11*, 1249–1267. [CrossRef]
49. Hack, E.; Lin, X.; Patterson, E.A.; Sebastian, C.M. A reference material for establishing uncertainties in full-field displacement measurements. *Meas. Sci. Technol.* **2015**, *26*, 75004. [CrossRef]

50. Landau, L.D.; Lifshitz, E.M.; Sykes, J.B.; Reid, W.H.; Dill, E.H. Theory of Elasticity: Vol. 7 of Course of Theoretical Physics. *Phys. Today* **1960**, *13*, 44–46. [CrossRef]
51. Breuer, K.; Stommel, M. RVE modelling of short fiber reinforced thermoplastics with discrete fiber orientation and fiber length distribution. *SN Appl. Sci.* **2020**, *2*, 140. [CrossRef]
52. Jackson, A.P.; Vincent, J.; Turner, R.M. The mechanical design of nacre. *Proc. R. Soc. Lond. B* **1988**, *234*, 415–440. [CrossRef]
53. Bekah, S.; Rabiei, R.; Barthelat, F. Structure, Scaling, and Performance of Natural Micro- and Nanocomposites. *BioNanoScience* **2011**, *1*, 53–61. [CrossRef]